† Electronic Supplementary Information (ESI)

Nitrogen-doped arch and hollow shaped nanocarbons for CO_2 adsorption.

Prakash Ramakrishnan, Sangaraju Shanmugam*

* Department of Energy Systems Engineering, Daegu Gyeongbuk Institute of Science & Technology (DGIST), 50^{-1} Sang-Ri, Hyeongpung-Myeon, Dalseong-gun, Daegu, 711-873, Republic of Korea.

Tel.: +82-53-785-6413. Fax: +82-53-785-6409.

E-Mail address: sangarajus@dgist.ac.kr

Experimental section

In a typical experiment, the nitrogen doped porous carbon nanostructures were prepared by following three simple steps: (1) Fabrication of core-shell fibrous membrane by coaxial electro spinneret with different flow rates, (2) Leaching out of core material through a simple hot water dipping and sonication process, (3) Stabilization and carbonization of leached fibrous membrane under air and argon atmosphere at different temperatures.

Fabrication of N-doped porous HCNR: The N-doped porous hollow carbon nanorods were prepared by co-axial electrospinning approach, prior to the experiment, PAN (Mw= 150,000 $gmol^{-1}$) of 10 wt% and PVP (Mw= 1,300,000 g mol^{-1}) of 20 wt% were added in 10 ml of *N,N*-dimethylformamide (DMF) separately and stirred at 80 ^{o}C, until a clear homogenous solution was obtained. The prepared two different homogeneous polymers were loaded into co-axial electrospinning syringes; PAN polymer solution in a pump1 syringe (P1, needle orifice of 0.86mm) which acts as a shell material or N source precursor and a PVP polymer solution in a pump2 syringe (P2, needle orifice of 0.26 mm) play as a core material or sacrificial material in this study. The following electrospinning parameters were adopted: the flow rate of P1 was kept at 0.1 ml h^{-1}, flow rate for P2 was kept at 0.5 ml h^{-1}, distance between the aluminum wrapped collector drum and the coaxial needle was set at 15 cm, a collector drum rotating speed of 300 rpm and a high voltage power supply of 13.5 kV under humidity < 30 % RH.

The as prepared electrospun membrane was cut into small pieces (2 x 2cm) and dipped in hot water at 75 ^{o}C for 12 h. Hot water was replaced every 3 h followed by sonication for 15 min and dried in oven for 10 min at 70 ^{o}C. The leached out membrane was stabilized at 250 ^{o}C for 2 h at a heating rate of 2 ^{o}Cmin^{-1} under air atmosphere and followed by carbonization under argon atmosphere at 800 ^{o}C for 1h at a heating rate of 5 ^{o}C min^{-1}. The carbonized product yield was found to be ~32%. The obtained product was ground using a mortar and pestle and labeled as HCNR.

Fabrication of N-doped porous ACNR: The N-doped arch shaped structure was prepared by following the same procedure of HCNR except that the flow rates of P1 and P2 was changed to 5 ml h^{-1} and 1 ml h^{-1}, respectively, thereby preparing arch shaped morphology and named as ACNR.

Fabrication of N-doped CNR comparison studies: For comparison, well known N-doped carbon nanorod structure was prepared by conventional electrospinning approach using a PAN solution of 10 wt% and followed by stabilization and carbonization with the temperature same as HCNR and ACNR. The obtained carbonized product of 36 % was ground using mortar and pestle and labeled as CNR.

Characterizations: The morphology was observed with field emission scanning electron microscope (S4800 FE-SEM) and field emission transmission electron microscope (HF 3600 FE-TEM). The phase and structure were carried out using high resolution X-ray diffraction (HR-XRD). The quantitative elemental analyses were measured using elemental analyzer (EA, Vario MICRI cube) and X-ray photo-electron spectroscope (XPS, Thermo scientific ESCALAB 250Xi). The surface area, microporous information, the microporous (0.5-2 nm) and mesoporous (2-50 nm) pore size distribution were determined by N_2 adsorption–desorption measurements (Micromeritics, ASAP 2020 at 77 K) using Bruner–Emmett–Teller (BET), the t-plot method (Harkins and Jura formula) and non-local density functional theory (NLDFT), respectively. In prior to measurements, the samples were degassed at 180 ^{o}C under vacuum overnight. The CO_2 adsorption isotherm measurement also done using Micromeritics ASAP 2020 at 273, 293, 298 and 303 K and before measurement all the samples were degassed at 180 ^{o}C under vacuum for 8h. The measurements under different temperatures and gases were taken consecutively without degassing. Circulating bath was provided to control the temperatures.

The formulae used for calculation:-

The isosteric heat of adsorption was calculated according to Clausius-Clapeyron equation:

$Q\text{st} = RT^2(\partial \ln P/\partial \text{T})q$

Where P is pressure, T is temperature, q is the amount adsorbed, R is the gas constant,

and Qst denotes the heat of adsorption.

The selectivity (S) for adsorption of CO_2 over N_2 was calculated from the ratio

of the adsorbed amount of CO_2 at 0.15 bar to the adsorbed amount of N_2 at 0.75 bar at constant temperature; the value is normalized for the pressures chosen, according to equation:

$S = (q\text{CO}_2/q\text{N}_2)/(p\text{CO}_2/p\text{N}_2)$

where q is the amount adsorbed and P is pressure.

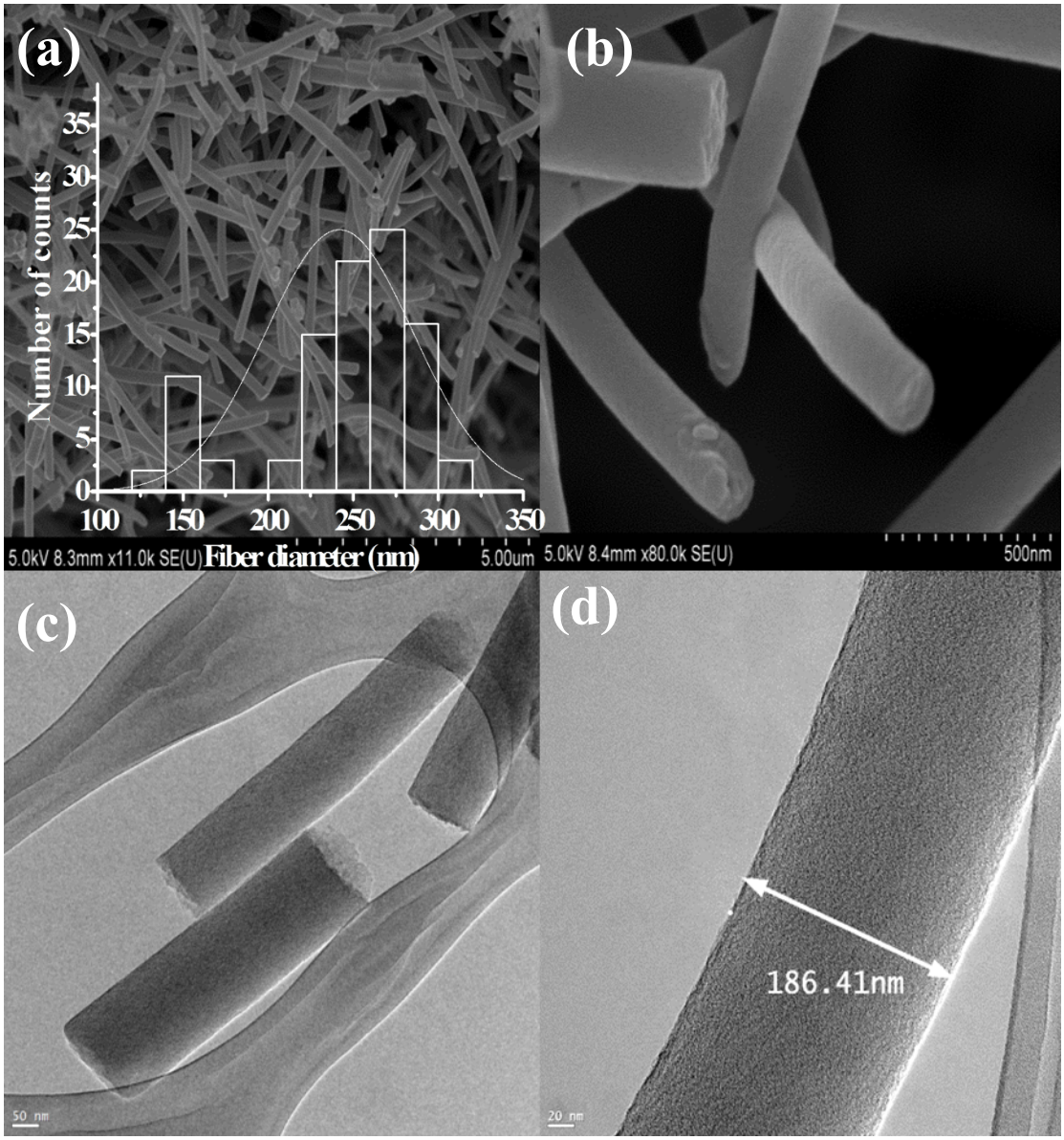

Fig.S1 (a, b) FE-SEM and (c, d) FE-TEM images of CNR sample.

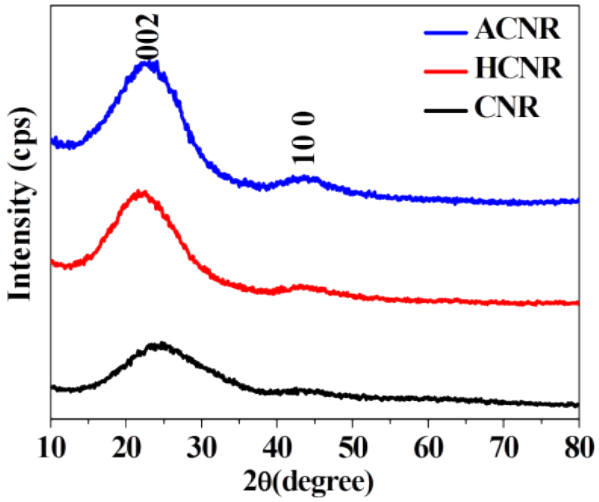

Fig. S2 XRD of CNR, HCNR and ACNR samples, respectively.

The XRD patterns of CNR, HCNR and ACNR exhibits similar features as shown in Figure S4a. The broad peaks observed at around 2θ = 24° and 44° are hexagonal graphitic carbon with (002) and (100) lattice planes, respectively. However, the broad graphite peaks observed in (002) and (100) represent the existence of N atoms in the carbon lattice which results partially amorphous in nature.[1] Particularly, a (002) plane widens due to the presence of N and fading of a lattice plane (1 0 0) attributed to the increase in N content, which clearly shows the existence of graphitic and turbostatic hybrid structures of carbon in all the samples.[2]

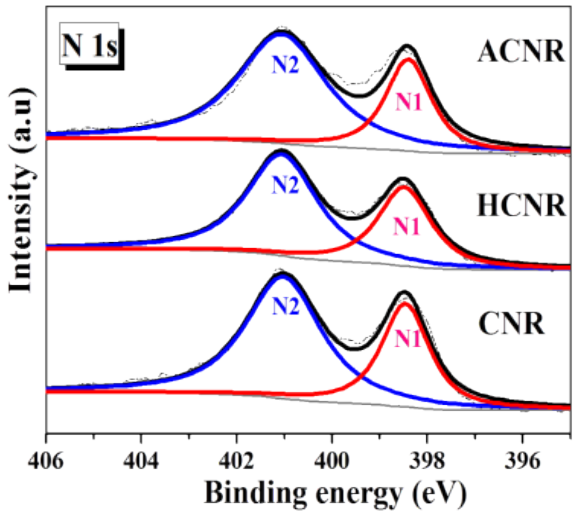

Fig. S3 High resolution N1s XPS spectra of CNR, HCNR and CNR samples, respectively.

The deconvoluted N 1s spectra (Fig. S3) of all the samples show pyridinic-N at N1 (398.4 ± 0.1 eV) and quaternary-N at N2 (401.0 ± 0.1 eV) (Table S1).[3] Moreover, these peaks are only symmetric without broadness and tail inference. So the possibility of other N-species are disregarded.

.

Table S1. XPS deconvuluted values of N_{1s} for all samples

Samples	N_{1s}	
	N_1 (eV)	N_2 (eV)
CNR	398.4	401.0
HCNR	398.5	401.1
ACNR	398.4	401.1

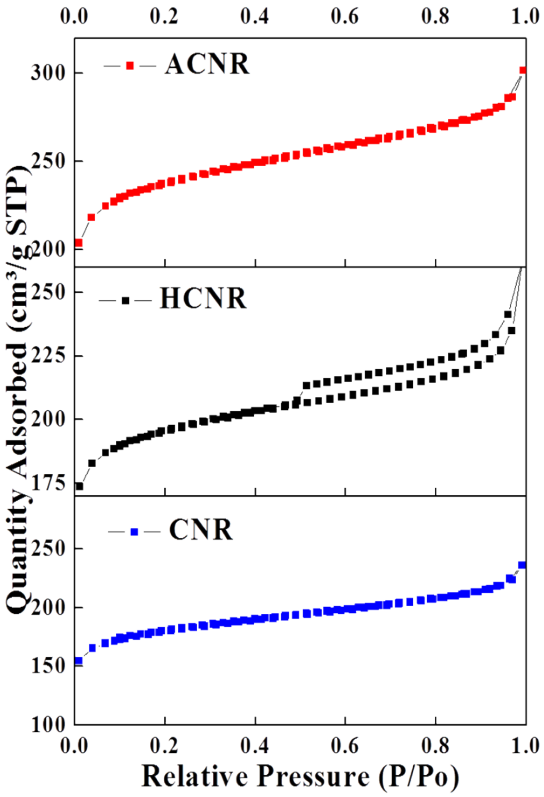

Fig. S4 BET absorption and desorption plots of all the samples.

The isotherms obtained for CNR and ACNR sample shows type I; HCNR sample displays both type I and type IV isotherm, as shown in Fig. S4. The differences in isotherm are due to differences in morphologies; especially the HCNR exhibits hysteresis isotherm from the partial pressure region of 0.45 to 1.0 due to presence of mesopore range (< 50nm) hollow structure; besides, the condensation of N_2 gas at high partial pressure region at 1.0 P/Po was due to the presence of macropores >50 nm as observed in FE-SEM and HR-TEM images in Fig. 1.

Table S2. Structural/textural properties of all samples determined using BET, T-plot and Nl-DFT methods.

Samples	S_{BET} [a] ($m^2.g^{-1}$)	$S_{t\text{-}plot}$ [b] ($m^2.g^{-1}$)	A_{Micro} [c] (%)	V_{micro} [d] ($cm^3.g^{-1}$)	V_{total} [e] ($cm^3.g^{-1}$)	P_{micro} [f] (nm)
CNR	484.1 ± 09	333.9	69.41	0.2125	0.4803	1.590
HCNR	556.9 ± 11	416.7	74.82	0.2415	0.5681	1.591
ACNR	619.3 ± 11	432.4	69.82	0.2852	0.6589	1.590

[a] S_{BET} : Specific surface area determined by BET method for P/P_0= 0.05 to 0.12.

[b] $S_{t\text{-}plot\text{-}internal}$: Microporous surface area determined by t-plot method using Harkins and Jura thickness equation.

[c] A_{Micro} : Percent of pore surface area contributed by micropores

[d] V_{micro} : Micropore volume was calculated using the t-plot method.

[e] V_{total} [f] P_{micro} : Total pore volume and width of the pore calculated using the NL-DFT.

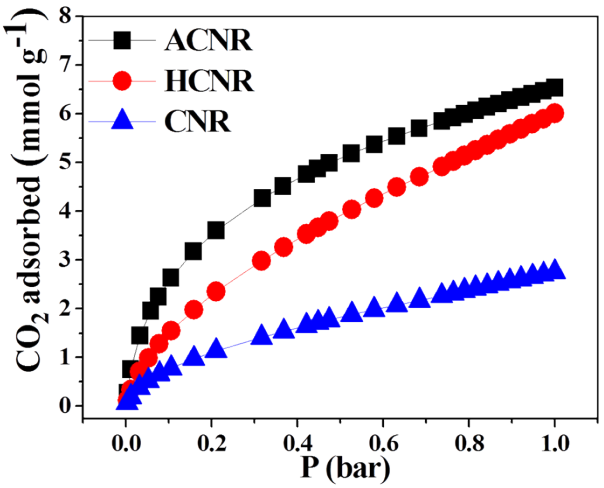
ACNR
HCNR
CNR
CO2 adsorbed (mmol g-1)
P (bar)
0
1
2
3
4
5
6
7
8
0.0
0.2
0.4
0.6
0.8
1.0

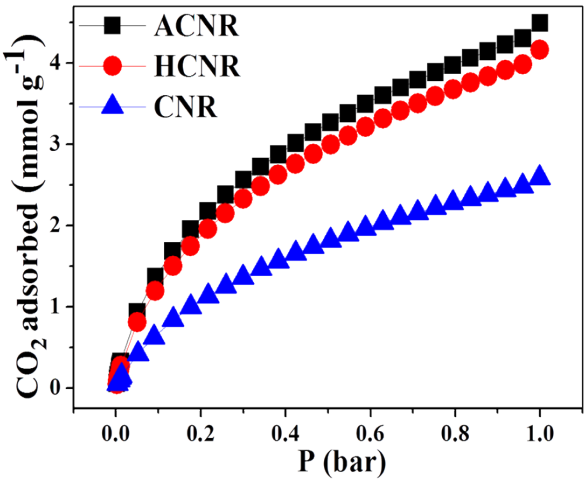
ACNR
HCNR
CNR
CO2 adsorbed (mmol g-1)
P (bar)
0
1
2
3
4
0.0
0.2
0.4
0.6
0.8
1.0

Fig. S5. CO_2 adsorption at 273 K (a), 293 K(b), 303 K (c) and Isosteric heat of CO_2 adsorption (d) calculated at 273, 293, 298 and 303 K for all samples CNR, HCNR and ACNR samples.

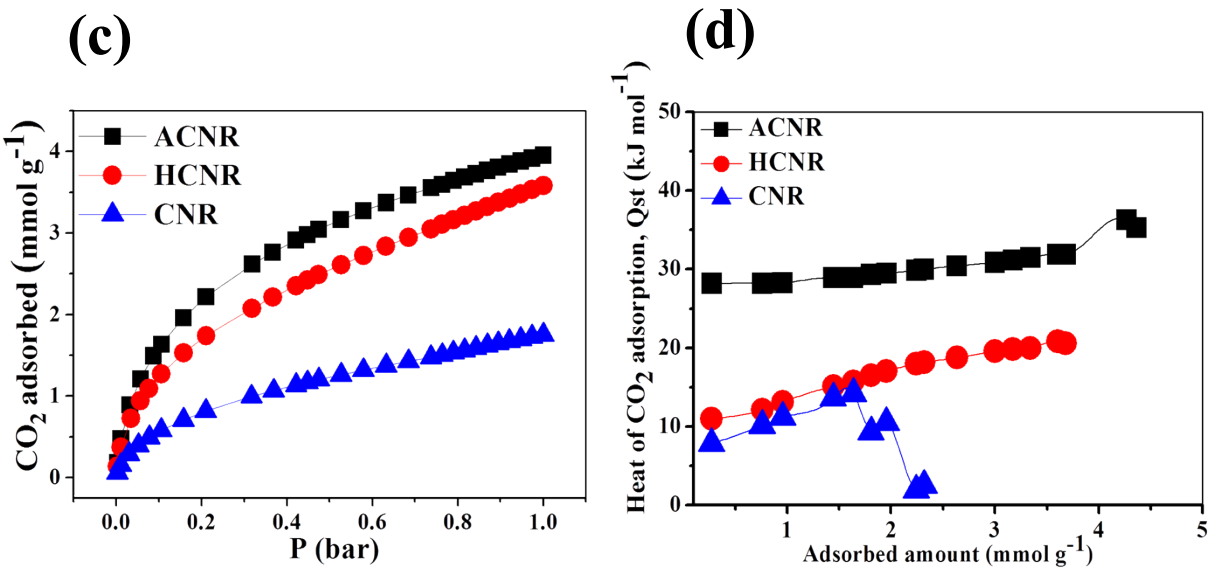

In Fig. S5d, the ACNR, HCNR and CNR sample follows differ heat of CO_2 gas adsorption due to the differences in textural properties such as BET surface area, T-plot micro-porous area, and pore volume (Table S2). Also, ACNR and HCNR shows' no saturation level in CO_2 adsorption as well as in heat of adsorption studies, which clearly conveys both of them are potentially suitable for CO_2 adsorption at elevated pressure.

Table S3. Comparison of previous reports on N-doped carbon materials in CO_2 adsorption studies.

Adsorbents (N-doped/N-free carbon materials)	**N (wt%)**	**Surface area (m^2 g^{-1})**	**CO_2 adsorption, 1 bar at 298 K (mmol g^{-1})**	**Ref.**
N-carbon molecular sieves	5.4	349	2.7	4
N- porous carbon	2.7	2747	3.9	5
N-hollow carbon	14.8	767	2.67	6
N-porous carbon	6.73	1979	4.3	7
N-microporous carbon	5.58	263	1.95	8
N-KOH activated PPy carbon	10.1	1700	3.90	9
N-porous carbon	4.8	1360	4.3	10
N-porous carbon monolithic	1.92	467	3.13	11
N-activated carbon	2.22	2596	3.75	12
Microporous carbon	Nil	808	3.8	13
Monolithic porous carbon	Nil	1935	4.2	14
Ultra-micro porous carbon	Nil	1220	3.97	15
Carbon aerogels	Nil	1100	**2.2**	16
N-HCNR	8.22	~556	**3.75**	This work

N-ACNR	8.70	~619	**4.23**	This work

Supporting information references:

1. H. Chen, F. Sun, J. Wang, W. Li, W. Qiao, L. Ling, and D. Long, *J. Phys. Chem. C*, 2013, **117**, 8318–28.

2. N. Iwashita, C. R. Park, H. Fujimoto, M. Shiraishi, and M. Inagaki, *Carbon*, 2004, **42**, 701–714.

3. S. R. Kelemen, M. L. Gorbaty, and P. J. Kwiatek, *Energy & Fuels*, 1994, **8**, 896–906.

4. J. Patiño, M. C. Gutiérrez, D. Carriazo, C. O. Ania, J. L. G. Fierro, M. L. Ferrer, and F. del Monte, *J. Mater. Chem. A*, 2014, **2**, 8719-29.

5. A. Aijaz, N. Fujiwara, and Q. Xu, *J. Am. Chem. Soc.*, 2014, **136**, 6790–3.

6. S. Feng, W. Li, Q. Shi, Y. Li, J. Chen, Y. Ling, A. M. Asiri, and D. Zhao, *Chem. Commun.,* 2014, **50**, 329–31.

7. X. Ma, M. Cao, and C. Hu, *J. Mater. Chem. A*, 2013, **1**, 913-8.

8. J. Wang, I. Senkovska, M. Oschatz, M. R. Lohe, L. Borchardt, A. Heerwig, Q. Liu, and S. Kaskel, *ACS Appl. Mater. Interfaces*, 2013, **5**, 3160–7.

9. M. Sevilla, P. Valle-Vigón, and A. B. Fuertes, *Adv. Funct. Mater.*, 2011, **21**, 2781–7.

10. V. Chandra, S. U. Yu, S. H. Kim, Y. S. Yoon, D. Y. Kim, A. H. Kwon, M. Meyyappan, and K. S. Kim, *Chem. Commun.*, 2012, **48**, 735–7.

11. G.-P. Hao, W.-C. Li, D. Qian, and A.-H. Lu, *Adv. Mater.*, 2010, **22**, 853–7.

12. Z. Zhang, M. Xu, H. Wang, and Z. Li, *Chem. Eng. J.*, 2010, **160**, 571–7.

13. D. Qian, C. Lei, E.-M. Wang, W.-C. Li, and A.-H. Lu, *ChemSusChem*, 2014, **7**, 291–8.

14. L. Estevez, R. Dua, N. Bhandari, A. Ramanujapuram, P. Wang, and E. P. Giannelis, *Energy Environ. Sci.*, 2013, **6**, 1785-90.

15. J. Cai, J. Qi, C. Yang, and X. Zhao, *ACS Appl. Mater. Interfaces*, 2014, **6**, 3703–11.

16. E. Masika and R. Mokaya, *RSC Adv.*, 2013, **3**, 17677-81.